



## Direct electrolytic preparation of chromium metal in $\text{CaCl}_2\text{--NaCl}$ eutectic salt

Zheng-wei LIU<sup>1,2,3</sup>, Hong-ling ZHANG<sup>1,2</sup>, Li-li PEI<sup>1,2</sup>, Yi-lang SHI<sup>4</sup>, Zai-hua CAI<sup>4</sup>, Hong-bin XU<sup>1,2</sup>, Yi ZHANG<sup>1,2</sup>

1. CAS Key Laboratory of Green Process and Engineering, Institute of Process Engineering, Chinese Academy of Sciences, Beijing 100190, China;
2. National Engineering Laboratory for Hydrometallurgical Cleaner Production Technology, Institute of Process Engineering, Chinese Academy of Sciences, Beijing 100190, China;
3. University of Chinese Academy of Sciences, Beijing 100049, China;
4. Hubei Zhenhua Chemical Co., Ltd., Huangshi 435001, China

Received 16 November 2016; accepted 20 April 2017

**Abstract:** The electro-reduction of chromium oxide ( $\text{Cr}_2\text{O}_3$ ) was investigated in an equimolar mixture of  $\text{CaCl}_2\text{--NaCl}$  molten salt at 800 °C for developing a more efficient process for chromium preparation. Cyclic voltammetry and potentiostatic electrolysis were used to study the electro-reduction of the  $\text{Cr}_2\text{O}_3$ -loaded metallic cavity electrode. In addition, a number of parameters affecting the rate and extent of  $\text{Cr}_2\text{O}_3$  electrolysis were considered to better understand the electrolysis process. The results demonstrate that  $\text{CaCl}_2\text{--NaCl}$  molten salt is applicable for preparing Cr directly from  $\text{Cr}_2\text{O}_3$  and the electrolysis parameters exert great influence on the cathode product. Under optimal experimental conditions, nodular Cr with an oxygen content of 0.5% (mass fraction) was obtained without any chromium carbides detected by XRD. Furthermore, the relatively high solubility of CaO and quite rapid crystal growth result in the formation of large platelet  $\text{CaCr}_2\text{O}_4$ , and the addition of NaCl to  $\text{CaCl}_2$  results in several variations on the electrolysis process and the product morphology from pure  $\text{CaCl}_2$  molten salt.

**Key words:** electrolysis; chromium; chromium oxide;  $\text{CaCl}_2\text{--NaCl}$  molten salt

### 1 Introduction

Chromium (Cr) metal is an attractive engineering material for many areas of applications owing to its properties of high melting point and considerable corrosion resistance [1,2]. Cr metal is predominantly produced by aluminothermic reduction of  $\text{Cr}_2\text{O}_3$  at high temperature above the melting point of Cr. The other process is to use  $\text{CrO}_3$  aqueous electrolyte electrolysis. However, the side reactions, chiefly the redox cycling of the multi-valence chromium ions (mainly  $\text{Cr}^{2+}$ ,  $\text{Cr}^{3+}$  and  $\text{Cr}^{6+}$ ) and  $\text{Cr}^{3+}/\text{Cr}$  electrode potential being more negative than that of  $\text{H}^+/\text{H}_2$ , account for the low current efficiency and the hydrogen brittleness [3]. In addition, there are laboratory studies about Cr electro-deposition from expensive  $\text{CrCl}_2$ ,  $\text{CrCl}_3$  or  $\text{K}_3\text{CrF}_6$  in molten salt [3–5].

The FFC-Cambridge process, based on the concept of cathodic oxygen ionization of solid oxide in  $\text{CaCl}_2$ -based molten salt, has been demonstrated for the

successful preparation of metals and alloys, such as titanium [6–9], niobium [10,11], tantalum [12,13], silicon [14], germanium [15], zirconium [16,17],  $\text{CeCo}_5$  [18], and  $\text{ZrMn}_5$  [19]. Particularly, researchers have validated the feasibility of the electro-reduction of  $\text{Cr}_2\text{O}_3$ , and a series of experiments have been performed to determine the influence of the electrolysis time, electrolysis voltage and anode areas on the electrolysis process in  $\text{CaCl}_2$  molten salt [1,2,20]. However, pure  $\text{CaCl}_2$  has a high melting point of 782 °C, hence, resulting in the electrolysis temperature as high as 900–950 °C. Moreover, chromium carbide was detected after  $\text{Cr}_2\text{O}_3$  electrolysis due to the high temperature and high solubility of  $\text{O}^{2-}$  in  $\text{CaCl}_2$  molten salt [20,21]. A process is always desired if it can proceed without external heating or at a lower temperature, if heating is inevitable, because of its relative energy-saving, mild reaction conditions and reduced corrosion property [10]. Substitutional  $\text{CaCl}_2$ -based electrolyte with low melting temperature has been selected to perform the FFC

process. For instance, it is demonstrated experimentally that  $\text{CaCl}_2\text{-NaCl}$  eutectic salt as the electrolyte is available and could be applied to preparing Nb [10], Ta [12], Ge [15], and U [22]. The addition of NaCl or other alkali or alkaline earth chloride to  $\text{CaCl}_2$  may affect the electrolysis of solid oxide in several manners: both desired and undesired [2]. GORDO et al [2] reported that  $\text{CaCl}_2\text{-NaCl}$  molten salt is expected to have a lower capability to accommodate  $\text{O}^{2-}$ , leading to a lower background current and alleviative graphite corrosion.

Herein, the equimolar mixture of  $\text{CaCl}_2$  and NaCl was selected as the molten salt. CVs and potentiostatic electrolysis of  $\text{Cr}_2\text{O}_3$  in  $\text{CaCl}_2\text{-NaCl}$  molten salt were investigated. Experimental work was also undertaken to study the influence of process variables on the extent and rate of electro-reduction of  $\text{Cr}_2\text{O}_3$ . Particular attention was paid to the role of  $\text{Ca}^{2+}$  and  $\text{Na}^+$  involved in the formation of intermediate product, because intermediate  $\text{Ca}_x\text{M}_y\text{O}_z$  (M means metal) was often detected, whereas  $\text{Na}_x\text{M}_y\text{O}_z$  was rarely found during the electrolysis of metal oxides in  $\text{CaCl}_2\text{-NaCl}$  molten salt [10,12,15,22]. Finally, the influence of  $\text{CaCl}_2\text{-NaCl}$  and pure  $\text{CaCl}_2$  on the electrolysis process and the product morphology was compared.

## 2 Experimental

$\text{Cr}_2\text{O}_3$  (>99%, mass fraction) powders of 1.5 g were compressed into compact cylinder pellet with a uniaxial pressure of 170 MPa in a 13 mm diameter steel die. These pellets were subsequently sintered at a specific temperature for 3 h. The porosity of the as-sintered pellet was measured by the Archimedes method. The sintered pellets were then drilled, connected into a current collector and assembled as an oxide cathode. Anhydrous  $\text{CaCl}_2$  (>96%, mass fraction) and NaCl (>99.5%, mass fraction) were blended with mole ratio of 1:1 in alumina crucible (99%, mass fraction). The details of the preparation for the electrolyte were described in Ref. [10].

CV curves of  $\text{Cr}_2\text{O}_3$  in  $\text{CaCl}_2\text{-NaCl}$  molten salt were recorded using the metallic cavity electrode (MCE) according to Ref. [23], with a computer-assisted solartron electrochemical workstation employed.  $\text{Cr}_2\text{O}_3$  powders were manually pressed into the cavity of the MCE, which functioned as working electrode during CV test. A graphite rod and  $\text{Ag/Ag}^+$  electrode (10%  $\text{AgCl}$ , 45% NaCl and 45% KCl in mole fraction, sealed in alumina pipe) were used as the counter and reference electrodes, respectively [24]. The CV tests were conducted with a scan rate of 100 mV/s, with the potential ranging from 0 to  $-1.8$  V (vs  $\text{Ag/Ag}^+$ ). Potentiostatic electrolysis was performed at  $-1.4$  V (vs  $\text{Ag/Ag}^+$ ) using MCE loaded with  $\text{Cr}_2\text{O}_3$ . After

potentiostatic experiment for 300 s, the  $\text{Mo/Cr}_2\text{O}_3$  sample was retrieved, washed with dilute HCl solutions and dried.

The electrolysis of solid  $\text{Cr}_2\text{O}_3$  was performed in a sealed stainless steel reactor, in which the center was located in the alumina crucible holding the molten salt. A high-density graphite rod of 15 mm in diameter was used as the anode. Both the anode and cathode current collectors were enclosed by an alumina pipe for insulation. The cell was flushed with argon while it was heated to the required temperatures and kept leak-proof to maintain an inert atmosphere of high purity argon gas. On reaching electrolysis temperature of  $800$  °C, the pre-electrolysis of the thermally dried molten salt was conducted using a constant voltage of 2.0 V applied between the graphite anode and stainless steel cathode to remove the residue moisture and metallic impurities from the electrolyte. After pre-electrolysis,  $\text{Cr}_2\text{O}_3$  electrode was inserted into the molten salt and a constant voltage varying from 2.5 to 3.2 V was imposed between the anode and oxide cathode with approximately 30 mm apart from each other. The graphite anode was immersed to a salt depth of 3 cm corresponding to a geometric surface area of  $16$  cm<sup>2</sup>. After a predetermined time, the electrolysis was terminated and the cathode was quickly lifted above the molten salt, cooled in argon atmosphere to room temperature and removed from the reactor. These recovered pellets were subsequently washed with distilled water to remove the solidified salt. They were further rinsed with dilute HCl solutions with pH 3. Such vigorous procedure could confirm that all the salts attached on the pores of the pellets could be eliminated from the electrolysis product. Finally, the sample was dried in a freezer dryer.

The microstructural composition of the sintered or electrolyzed pellet was observed using a scanning electron microscope (SEM) coupled with an energy-dispersive X-ray analysis (EDXA) attachment. Various phase compositions present in the prepared samples were determined by X-ray diffraction (XRD) with the scan range set from  $10^\circ$  to  $90^\circ$  after grinding the pellet. The oxygen content was determined by pulsed infrared melting-infrared thermal conductivity detection analysis (PIM-ITC).

## 3 Results and discussion

### 3.1 Electrochemical test

$\text{CaCl}_2\text{-NaCl}$  eutectic salt with mole ratio of 1:1 has a low melting point of  $504$  °C, whereas most-frequently used  $\text{CaCl}_2$  has a high melting point of  $782$  °C, thus giving the eutectic salt potential to be employed at a lower working temperature. Table 1 illustrates the theoretical electrode potentials of  $\text{Cr}_2\text{O}_3$ ,  $\text{CaCl}_2$  and NaCl

at 800 °C. As can be evidently observed, the theoretical decomposition potential of  $\text{Cr}_2\text{O}_3$  is far less than that of individual pure salt  $\text{CaCl}_2$  and  $\text{NaCl}$ . Attention should be especially paid to the calcium chromite ( $\text{CaCr}_2\text{O}_4$ ), which is believed to be an intermediate product during the electrolysis of  $\text{Cr}_2\text{O}_3$  [1,2,25]. The theoretical decomposition potential is higher than that of  $\text{Cr}_2\text{O}_3$ , but still lower than that of individual salt. Thus, thermodynamically applicable  $\text{CaCl}_2$ – $\text{NaCl}$  eutectic salt could be employed as the molten salt electrolyte when voltage of 2.5–3.2 V in this context is applied between the oxide cathode and graphite anode. Besides,  $\text{CaCl}_2$ – $\text{NaCl}$  eutectic salt has a higher electrical conductivity and lower viscosity compared to  $\text{CaCl}_2$  molten salt, providing a better flow field environment for the electrolysis.

**Table 1** Electrochemical properties of selected chromium compounds and chlorides at 800 °C with reference to  $\text{Ca}^{2+}/\text{Ca}$  couple

Reaction	$\varphi/\text{V}$
$\text{Cr}_2\text{O}_3 + 6\text{e} = 2\text{Cr} + 3\text{O}^{2-}$	1.235
$\text{CaCr}_2\text{O}_4 + 6\text{e} = 2\text{Cr} + \text{Ca}^{2+} + 4\text{O}^{2-}$ (900 °C)	0.778
$2\text{Cl}^- = \text{Cl}_2 + 2\text{e}$	3.292
$\text{O}_2 + 2\text{e} = \text{O}^{2-}$	2.709
$\text{O}^{2-} + \text{C} = \text{CO} + 2\text{e}$	1.637
$2\text{O}^{2-} + \text{C} = \text{CO}_2 + 2\text{e}$	1.683
$\text{Na}^+ + \text{e} = \text{Na}$	0.055
$\text{Ca}^{2+} + 2\text{e} = \text{Ca}$	0

The electrochemical behavior of  $\text{Cr}_2\text{O}_3$  in  $\text{CaCl}_2$ – $\text{NaCl}$  molten salt at 800 °C was investigated by CV measurement and potentiostatic electrolysis. Figure 1 presents the CV curves of blank MCE (solid line) and MCE loaded with  $\text{Cr}_2\text{O}_3$  (dash line) in  $\text{CaCl}_2$ – $\text{NaCl}$  molten salt. Peak C1 is the only peak observed in the CV curves of blank MCE and hence could be attributed to the cathodic formation of Ca and/or Na in  $\text{CaCl}_2$ – $\text{NaCl}$  molten salt. However, after loading  $\text{Cr}_2\text{O}_3$  into MCE, one additional reduction peak at –1.4 V (peak C2) is detected during the negative scan. As a result, peak C2 is ascribed to the electro-reduction of solid  $\text{Cr}_2\text{O}_3$  since peak C2 is the only cathodic peak detected after loading  $\text{Cr}_2\text{O}_3$  into MCE. Theoretically, the electro-reduction potential of  $\text{Cr}_2\text{O}_3$  is about 1.235 V higher vs  $\text{Ca}^{2+}/\text{Ca}$  (or 1.18 V vs  $\text{Na}^+/\text{Na}$ ). The narrow gap between the  $\text{Cr}_2\text{O}_3$  and  $\text{Ca}^{2+}/\text{Ca}$  reduction potential (Fig. 1) elucidates a high overvoltage necessitated to advance the  $\text{Cr}_2\text{O}_3$  electro-reduction. Actually, similar high overvoltage was observed during the CV test of  $\text{Cr}_2\text{O}_3$  in  $\text{CaCl}_2$  molten salt at 900 °C [23]. Potentiostatic electrolysis of  $\text{Cr}_2\text{O}_3$  was then performed at –1.4 V (vs  $\text{Ag}/\text{Ag}^+$ ). The SEM image of the product

from the potentiostatic electrolysis of MCE loaded with  $\text{Cr}_2\text{O}_3$  powders in  $\text{CaCl}_2$ – $\text{NaCl}$  molten salt at 800 °C for 300 s displays nodular particles of 200 nm in Fig. 2. The EDXA result confirms that the nodular particles are Cr metal with residue oxygen.

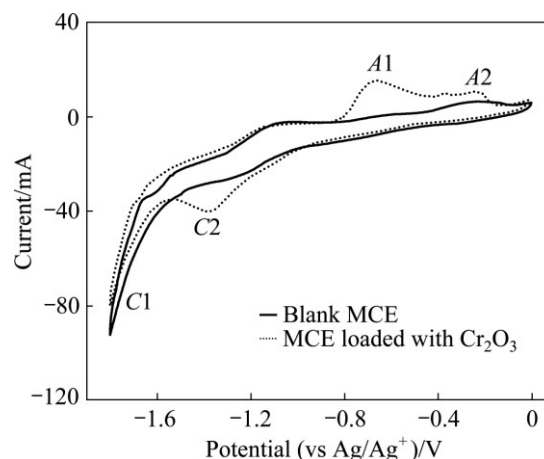


**Fig. 1** CV curves of blank MCE and MCE loaded with  $\text{Cr}_2\text{O}_3$  in  $\text{CaCl}_2$ – $\text{NaCl}$  molten salt at 800 °C and scan rate of 100 mV/s

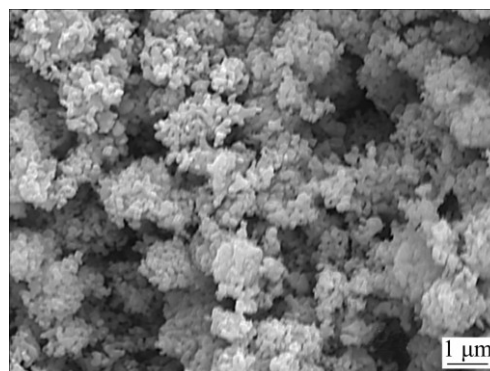


**Fig. 2** SEM image of product from potentiostatic electrolysis (–1.4 V (vs  $\text{Ag}/\text{Ag}^+$ )) of MCE loaded with  $\text{Cr}_2\text{O}_3$  in  $\text{CaCl}_2$ – $\text{NaCl}$  molten salt at 800 °C for 300 s

### 3.2 Influence of sintering temperature

Figure 3 shows the SEM images of the fracture surface of  $\text{Cr}_2\text{O}_3$  pellet sintered at different temperatures, from which the temperature dependence of the microstructures is clearly observed, especially at high sintering temperatures. The particles of the pellet exhibit an increase in size as the sintering temperature is raised from 1100 to 1400 °C [2]. As reported, the  $\text{O}^{2-}$  generated at the oxide cathode first proceeded across the particle in the solid form, followed by its diffusion through the pores of the cathode and finally reached the anode where  $\text{O}^{2-}$  was oxidized to  $\text{CO}/\text{CO}_2$  [26]. Thus, it would be reasonably speculated that  $\text{O}^{2-}$  would take a longer distance to diffuse to the particle's outer surface from the inside for the pellet with larger size distribution or sintered at higher temperature. Although the pellets sintered at different temperatures have a similar porosity

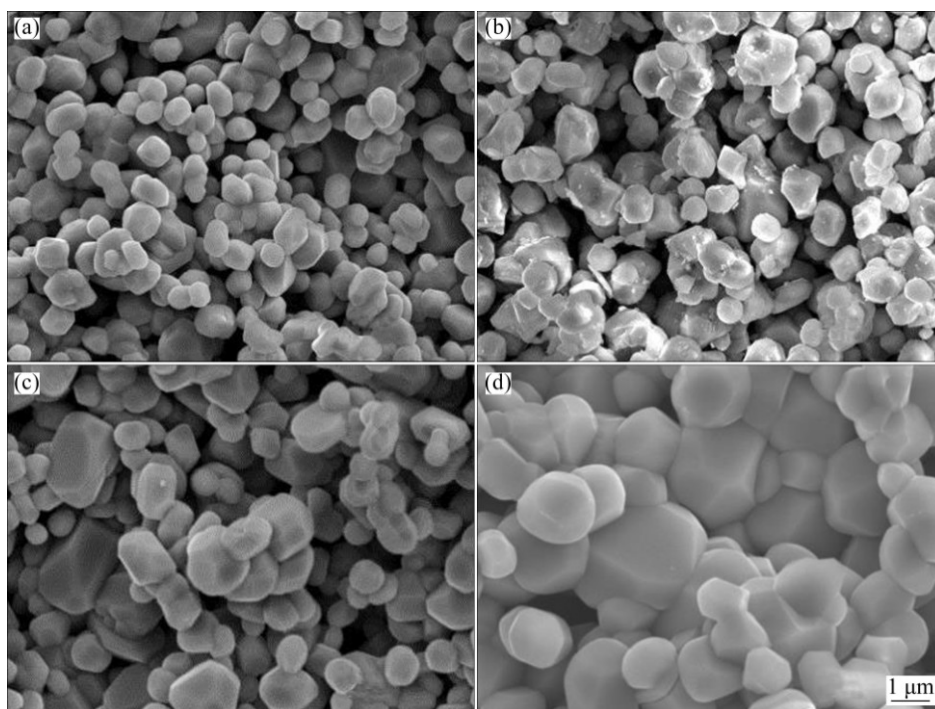


**Fig. 3** SEM images of cross sections of  $\text{Cr}_2\text{O}_3$  pellets sintered at different temperatures: (a) 1100 °C; (b) 1200 °C; (c) 1300 °C; (d) 1400 °C

of about 35%, the boundary between  $\text{Cr}_2\text{O}_3$  particles is more closely connected to each other at higher sintering temperatures. Therefore, there would be a compromise for  $\text{O}^{2-}$  diffusion rate due to the enlarged diffusion distance and the dense structure as a result of increased sintering temperature. Figure 4 shows the XRD patterns of cathode pellets subjected to electrolysis at an applied voltage of 3.0 V for 8 h, which demonstrates that the cathode pellet, sintered at lower temperature or with smaller size distribution, could be totally electrolyzed to Cr metal. In contrast, the cathode pellet sintered at higher temperature could only be partially electrolyzed as intermediate product  $\text{CaCr}_2\text{O}_4$  still remains. Accordingly, Figs. 5(a) and (b) show SEM images of the electrolysis products at sintering temperatures of 1100 and 1400 °C, respectively. The particles in Fig. 5(a) show uniformly nodular morphology of around 500 nm, which are confirmed to be Cr metal by EDXA result. The particles in Fig. 5(b) display two obviously dissimilar microstructures, being nodular and irregular morphologies. In combination of the XRD result (Fig. 4), the irregular morphology is believed to be  $\text{CaCr}_2\text{O}_4$  [1,2]. As a result, increasing the sintering temperature slows down the overall electrolysis rate to some extent and leads to partial oxygen removal from the cathode under the present experimental condition. The complete electrolysis of the oxide cathode, namely the highest electrolysis rate of  $\text{Cr}_2\text{O}_3$  pellet observed in Fig. 5(a), is hence attributed to the smaller particle size of  $\text{Cr}_2\text{O}_3$  pellet sintered at low temperature of 1100 °C, which

means that mass transfer of  $\text{O}^{2-}$  across the particle in the solid form is the rate-controlling step. Therefore, small particles are preferably employed in order to fulfill a complete electrolysis, while larger particles should be tried best to avoid, on account of not only decreasing the sintering temperature but also accelerating the rate of the electrolysis.

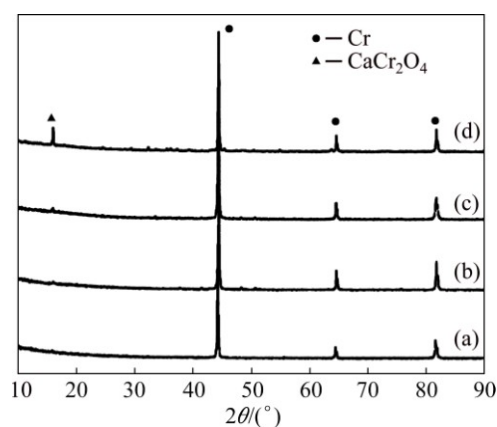


**Fig. 4** XRD patterns of electrolysis product at 3.0 V for 8 h and sintered at different temperatures: (a) 1100 °C; (b) 1200 °C; (c) 1300 °C; (d) 1400 °C

### 3.3 Influence of electrolysis voltage

The electro-reduction of  $\text{Cr}_2\text{O}_3$  pellet under varying voltages from 2.5 to 3.2 V for 8 h was conducted. The pellets used were prepared by die-pressing and sintered at 1100 °C for 3 h. The typical current–time behaviors at different voltages are presented in Fig. 6. The currents

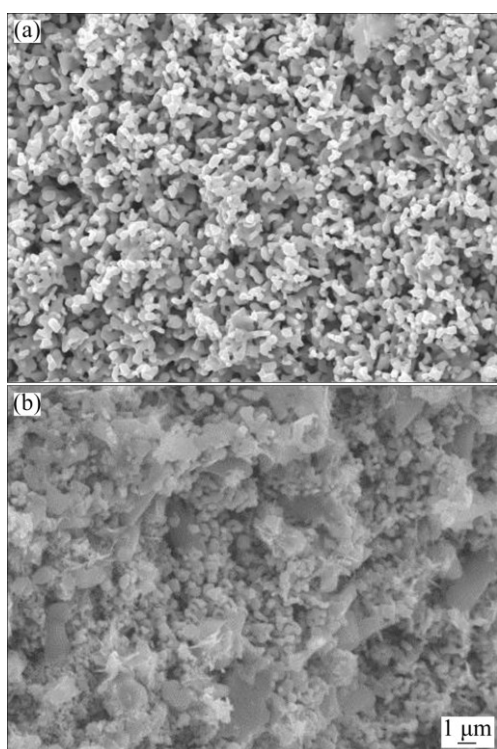


**Fig. 5** SEM images of electrolysis product at 3.0 V for 8 h and sintered at different temperatures: (a) 1100 °C; (b) 1400 °C

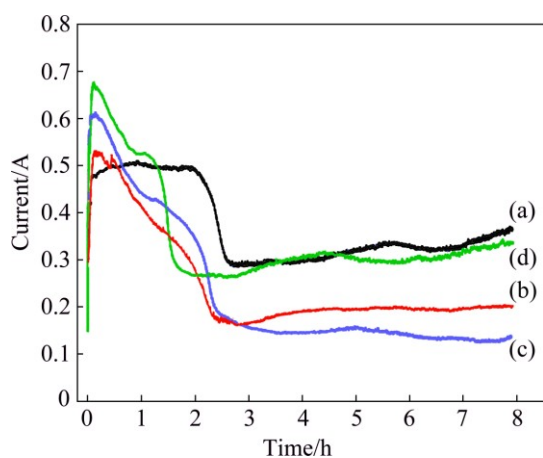


**Fig. 6** Current–time plots at different voltages between cathode and anode: (a) 2.5 V; (b) 2.8 V; (c) 3.0 V; (d) 3.2 V

recorded at 2.8, 3.0 and 3.2 V show similar features. Initially, it quickly reaches current peak and then gradually decays to the background current. The exception is the electrolysis of  $\text{Cr}_2\text{O}_3$  pellet at 2.5 V, the lowest applied voltage in this work. The recorded current quickly reaches initial current peak, but the current plateau endures for a longer time. The current at later stage is higher than that at higher voltage. According to the metal/oxide/electrolyte interface (3PI) theory [1], it may be the slow 3PI propagation toward the inside of pellet that causes long-time current plateau at low applied voltage of 2.5 V. Besides, the oxygen content of

the electrolysis product measured by PIM-ITC method is determined to be high about 9% (mass fraction), demonstrating an incomplete electrolysis. The incomplete electrolysis of  $\text{Cr}_2\text{O}_3$  might lead to the high current at later stage. Figure 7 shows the XRD patterns of the products after electrolysis at different voltages, indicating that voltage of 2.5 V is high enough to electrolyze  $\text{Cr}_2\text{O}_3$  to Cr metal. However, the residual oxygen content is high (about 9%) as described in Fig. 8. When the electrolysis voltage increases to 3.2 V,  $\text{Cr}_2\text{O}_3$  is fully electrolyzed to Cr metal with oxygen content as low as 0.5% (mass fraction). In practice, the voltage applied between the cathode and anode is not entirely consumed between the graphite anode and  $\text{Cr}_2\text{O}_3$  cathode, if concentration polarization and voltage loss due to circuit resistance is taken into account. These results clarify that high voltage is crucial in order to accomplish a complete electrolysis of  $\text{Cr}_2\text{O}_3$  with low oxygen content, while low voltage could only realize partial oxygen removal. The SEM image of the product after electrolysis at 2.5 V in Fig. 9(a) exhibits that some

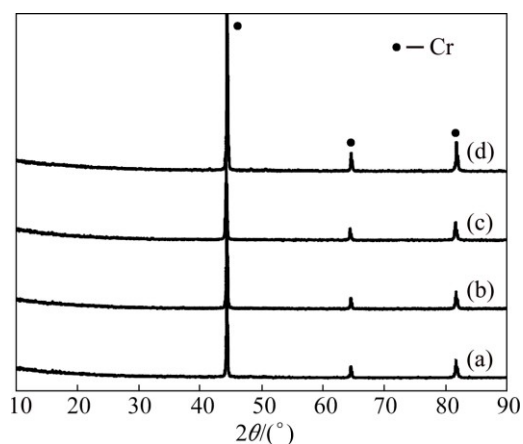


**Fig. 7** XRD patterns of electrolysis product at different voltages between cathode and anode for 8 h: (a) 2.5 V; (b) 2.8 V; (c) 3.0 V; (d) 3.2 V

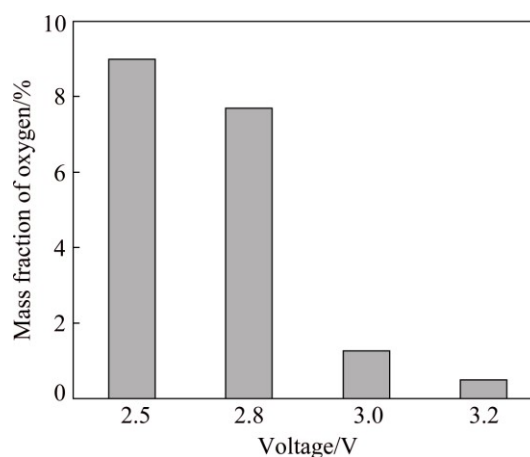


**Fig. 8** Residual oxygen content detected by PIM-ITC method at different voltages between cathode and anode

platelet morphologies are surrounded by nodular particles, of which the platelet morphologies are assigned to  $\text{CaCr}_2\text{O}_4$  and nodular particles of Cr metal [1,2,26], showing the incomplete electrolysis. In contrast, the SEM image of the product after electrolysis at 3.2 V in Fig. 9(b) displays nodular Cr particle morphology.

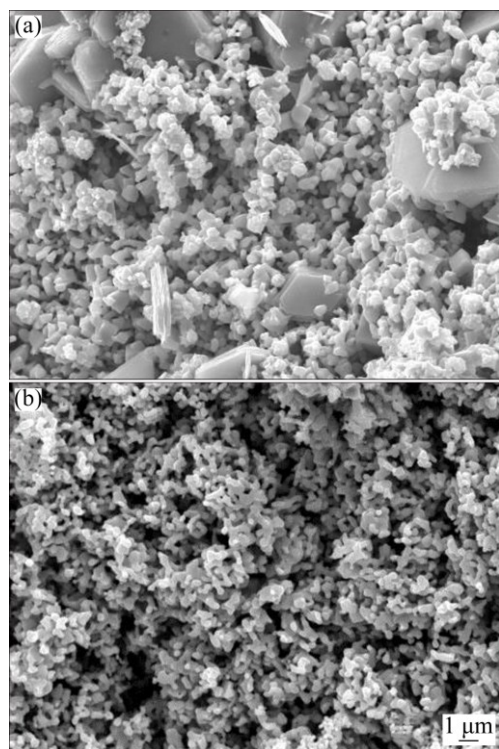


Fig. 9 SEM images of electrolysis product at different voltages between cathode and anode for 8 h: (a) 2.5 V; (b) 3.2 V

### 3.4 Influence of electrolysis duration

Figure 10 shows the XRD patterns obtained from specimens whose electrolysis was terminated after different periods of time from 0.25 to 8 h at 3.0 V. Sample obtained after electrolysis for 0.25 h is found to consist predominantly of  $\text{Cr}_2\text{O}_3$ . At the same time, metal Cr peak begins to show up, although Cr peak is quite minor. This could be attributed to little amount of Cr metal initially formed on 3PI interface. With the electrolysis process progressing, samples recovered for 0.5 and 1 h are primarily composed of  $\text{Cr}_2\text{O}_3$ , Cr and  $\text{CaCr}_2\text{O}_4$ . And samples retrieved at reaction time longer than 2 h contain mainly Cr metal, although there is small amount of  $\text{CaCr}_2\text{O}_4$ . Finally, the whole pellet turns to Cr metal after electrolysis for 8 h. In summary, with the electrolysis process progressing, the amount of  $\text{Cr}_2\text{O}_3$  gradually decreases and the amount of Cr rises, while  $\text{CaCr}_2\text{O}_4$  only exists temporarily as an intermediate.

$\text{CaCr}_2\text{O}_4$  with a diameter of micrometers is described above during the electrolysis of  $\text{Cr}_2\text{O}_3$  in  $\text{CaCl}_2$ -NaCl molten salt. However, no intermediate product such as  $\text{NaCrO}_2$  is detected. Likewise, similar phenomenon has been covered in the case of the

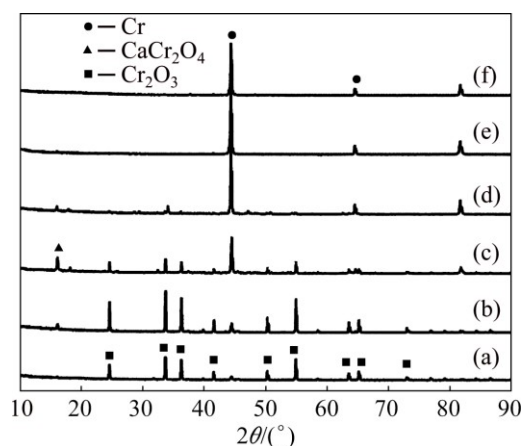
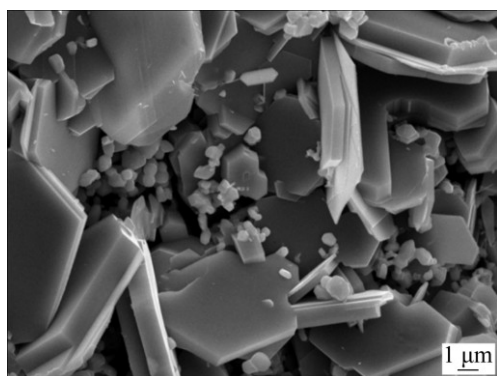


Fig. 10 XRD patterns of electrolysis product at 3.0 V for different time: (a) 0.25 h; (b) 0.5 h; (c) 1 h; (d) 2 h; (e) 4 h; (f) 8 h

electrolysis of other metal oxides, such as  $\text{Ta}_2\text{O}_5$ ,  $\text{Nb}_2\text{O}_5$ ,  $\text{GeO}_2$  in  $\text{CaCl}_2$ -NaCl molten salt. For instance, during the electrolysis process of  $\text{Nb}_2\text{O}_5$  to Nb in  $\text{CaCl}_2$ -NaCl molten salt,  $\text{Nb}_2\text{O}_5$  cathode undergoes several intermediate phases, such as  $\text{CaNb}_2\text{O}_6$ ,  $\text{CaNbO}_3$ ,  $\text{Ca}_2\text{Nb}_2\text{O}_7$ , and finally changes to Nb metal, whereas no  $\text{Na}_x\text{Nb}_y\text{O}_z$  compounds are detected [12,27]. In order to investigate the reason why no  $\text{NaCrO}_2$  compound is generated in  $\text{CaCl}_2$ -NaCl molten salt, experiment was conducted in pure NaCl molten salt at 900 °C with a applied voltage of 3.0 V between the anode and cathode. Only the very thin surface of the pellet turns to grey after electrolysis for 8 h, whereas the inside remains unchanged and resembles the starting precursor  $\text{Cr}_2\text{O}_3$ . This confirms that some mild reactions occur in pure NaCl molten salt, but only slightly. A typical SEM investigation obtained from the grey layer of partially electrolyzed pellet is presented in Fig. 11. Different morphologies of large platelets and small particles are observed. The EDXA results in Table 2 show that the large platelets are mainly composed of Cr, Ca, and O with small amount of Na detected. The presence of Ca detected by EDXA in the as-obtained product in pure NaCl molten salt is due to the impurity of analytical purity NaCl. Similarly, QIU et al [23] reported that the Mg observed by EDXA in the as-obtained product in pure  $\text{CaCl}_2$  molten salt is due to the impurity of analytical purity  $\text{CaCl}_2$ . Small particles are mainly composed of Cr and O, indicative of partial electrolysis of  $\text{Cr}_2\text{O}_3$ . So, it could be concluded that Ca plays a crucial role in the electrolysis process, while sodium exerts little influence on the process even in pure NaCl molten salt.

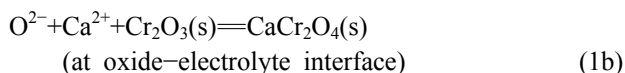
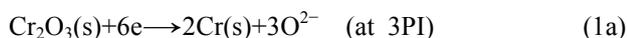
LIU et al [28] proposed the reaction pathway of the electro-reduction of  $\text{Cr}_2\text{O}_3$  to explain the mechanism for the generation of  $\text{CaCr}_2\text{O}_4$ .



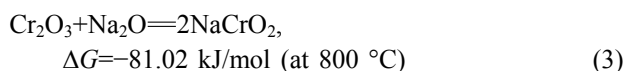
**Fig. 11** Typical SEM image of electrolysis product in NaCl molten salt

**Table 2** EDXA results of electrolyzed products in NaCl molten salt in Fig. 11

Element	Mole fraction/%	
	Small particle	Large platelet
O	23.22	55.75
Na	2.21	5.96
Ca	2.57	14.29
Cr	71.99	24.00



By analogy, the same mechanism proposed above could be applied to explaining the fact that the  $\text{NaCrO}_2$  forms in  $\text{CaCl}_2$ - $\text{NaCl}$  molten salt. As seen from Eqs. (2) and (3), the chemical reaction of  $\text{NaCrO}_2$  is much favorable than that of  $\text{CaCr}_2\text{O}_4$  from their respective oxides thermodynamically. However, the fact that no any  $\text{NaCrO}_2$  is found in the product runs counter to the thermodynamic prediction. There might be several reasons that lead to the phenomenon. The first is due to the low solubility of  $\text{Na}_2\text{O}$  dissolved in  $\text{CaCl}_2$ - $\text{NaCl}$  molten salt, which is disadvantageous for the formation of  $\text{NaCrO}_2$  according to Eq. (3). In comparison,  $\text{CaCl}_2$  could accommodate a reasonably large quantity of  $\text{CaO}$  (about 20%, mole fraction), which allows  $\text{O}^{2-}$  to dissolve in the molten salt [29]. Thus, the high solubility of  $\text{CaO}$  dissolved in the molten salt is favorable for the formation of  $\text{CaCr}_2\text{O}_4$ . The second could be attributed to  $\text{CaCr}_2\text{O}_4$  quick growth. In previous researches, ALEXANDER et al [7] reported that in the reaction of  $\text{TiO}$  with  $\text{CaTiO}_3$  to form  $\text{CaTi}_2\text{O}_4$ , rapid growth is the main reason behind the large size of  $\text{CaTi}_2\text{O}_4$  particles. In this context,  $\text{CaCr}_2\text{O}_4$  shows a typical morphology of large platelet of micrometers. Therefore, it would be reasonably assumed that  $\text{CaCr}_2\text{O}_4$  grows with a quite rapid crystal growth.



### 3.5 Comparison of molten salt medium

As discussed above, the addition of  $\text{NaCl}$  to  $\text{CaCl}_2$  salt alters the molten salt nature and affects the electrolysis of solid  $\text{Cr}_2\text{O}_3$  in a number of ways, desired and undesired. Several different features are easily observed from  $\text{CaCl}_2$  molten salt when  $\text{CaCl}_2$ - $\text{NaCl}$  molten salt is adopted as the electrolyte. Firstly, the background current at later stage of the electrolysis is much smaller than that in  $\text{CaCl}_2$  molten salt as predicted due to lower solubility of  $\text{O}^{2-}$  [20], thus a higher current efficiency becomes possible. Secondly, the final Cr particles possess the nodular morphology and have a size distribution ranging from 400 to 600 nm as displayed in Figs. 5(a) and 9(b). However, both nodular and cubic Cr particles were found during the electrolysis of  $\text{Cr}_2\text{O}_3$  in  $\text{CaCl}_2$  molten salt [1,2]. GORDO et al [2] reported that cubic Cr particles could be obtained if the electrolysis voltage is lower than 2.8 V. CHEN and FRAY [30] explained that the cubic Cr particles resulted from the preferential growth which could in principle convert the initial spherical nuclei or small crystallites into larger particles of cubic shapes. In  $\text{CaCl}_2$ - $\text{NaCl}$  molten salt, cubic Cr particles are never detected. Though the reason is not clear, it must be related to the eutectic salt providing a specific environment for the electrolysis of  $\text{Cr}_2\text{O}_3$ . The nodular Cr morphology is similar to that obtained in  $\text{CaCl}_2$  molten salt, except that the size is quite smaller than that 1–3  $\mu\text{m}$  obtained in  $\text{CaCl}_2$  molten salt, as shown in Fig. 12 [1,2,28]. This is attributed to the lower molten salt temperature of 800  $^\circ\text{C}$  applied under the experimental conditions as high temperature would result in sintering of Cr particles, which would allow the particles to grow into 1  $\mu\text{m}$  or larger in diameter in  $\text{CaCl}_2$  molten salt at 900  $^\circ\text{C}$ .  $\text{Cr}_2\text{O}_3$  is fully electrolyzed to Cr metal with oxygen content as low as 0.5% (mass fraction) at 3.2 V. In comparison with the oxygen content 0.2% (mass fraction) produced in  $\text{CaCl}_2$  molten salt, the oxygen content is a little higher [2,20,28]. Figure 13 shows a typical TEM image of the surface of Cr particles after electrolysis in  $\text{CaCl}_2$ - $\text{NaCl}$  molten salt. Clearly, a thin coating ( $\approx 5$  nm in thickness) is revealed and should be attributed to partial oxidation of the Cr surface. WU et al [11] reported similar oxide layer during the electro-reduction of  $\text{Nb}_2\text{O}_5$  to Nb metal. The coating is comparable in uniformity and might have formed during post-electrolysis processing operation including washing in water and exposure to air [11]. Assuming Cr particles to be spherical of 1  $\mu\text{m}$  in diameter and the oxide layer to be uniform with a similar thickness after electrolysis in

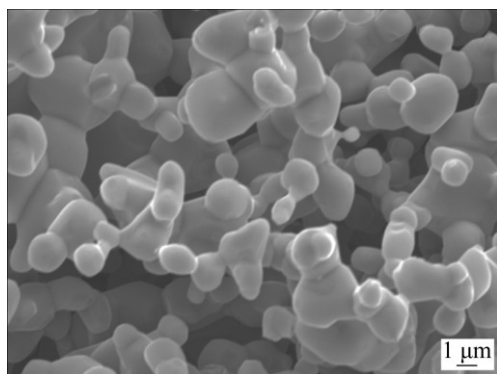


**Fig. 12** SEM image of nodular Cr product at 3.0 V for 8 h in  $\text{CaCl}_2$  molten salt at 900 °C

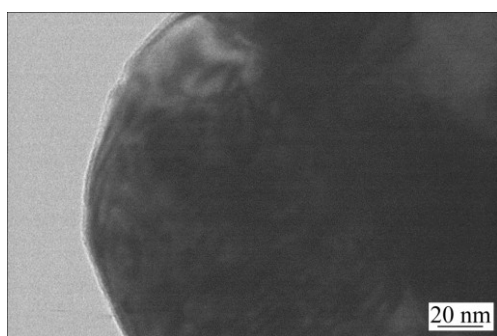


**Fig. 13** TEM image of electrolysis product at 3.2 V for 8 h between cathode and anode

$\text{CaCl}_2$  molten salt, the oxygen content of Cr metal produced in  $\text{CaCl}_2$ – $\text{NaCl}$  molten salt can be calculated to be twice higher than that produced in  $\text{CaCl}_2$  molten salt due to the small particle size distribution of 500 nm. This confirms a significant contribution of the oxide coating to the overall oxygen content in the electrolysis product. Thirdly, all peaks of the product after electrolysis could be assigned to Cr metal in Fig. 10(f). And no any chromium carbide is detected, denoting that  $\text{CaCl}_2$ – $\text{NaCl}$  molten salt with a lower working temperature could effectively avoid the carbon contamination. Herein, the lower temperature used not only reduces the corrosion of the graphite anode, but also decreases the chance of the chemical combination of Cr and C to form the chromium carbides.

## 4 Conclusions

1) CVs and potentiostatic electrolysis of MCE loaded with  $\text{Cr}_2\text{O}_3$  were studied to confirm the electro-reduction mechanism of rod-like  $\text{Cr}_2\text{O}_3$  to Cr at a potential of  $-1.40$  V (vs  $\text{Ag}/\text{Ag}^+$ ).

2) Metal Cr was successfully prepared from the electro-reduction of  $\text{Cr}_2\text{O}_3$  in the equimolar  $\text{CaCl}_2$ + $\text{NaCl}$ . The results indicated that Cr without chromium carbides detected could be achieved under the optimized conditions: pellet sintering temperature 1100 °C, voltage

3.2 V, duration 8 h. The as-obtained nodular Cr with oxygen content of 0.5% (mass fraction) has a diameter range from 400 to 600 nm.

3) It is assumed that the relatively high solubility of CaO and quite rapid crystal growth result in the formation of large platelet  $\text{CaCr}_2\text{O}_4$ . In comparison, no any  $\text{NaCrO}_2$  compounds are generated due to the low solubility of  $\text{Na}_2\text{O}$  in  $\text{CaCl}_2$ – $\text{NaCl}$  molten salt, although  $\text{NaCrO}_2$  is much more favorable to form thermodynamically.

## References

- [1] CHEN G Z, GORDO E, FRAY D J. Direct electrolytic preparation of chromium powder [J]. *Metall Mater Trans B*, 2004, 35: 223–233.
- [2] GORDO E, CHEN G Z, FRAY D J. Toward optimization of electrolytic reduction of solid chromium oxide to chromium powder in molten chloride salts [J]. *Electrochim Acta*, 2004, 49: 2195–2208.
- [3] MALYSHEV V V. Electrodeposition of chromium from ionic melts [J]. *Russ J Non-Ferr Met*, 2011, 52: 473–480.
- [4] COTARTA A, BOUTEILLON J, POIGNET J C, VASILIU F, COTARTA V. Preparation and characterization of chromium deposits obtained from molten salts using pulsed currents [J]. *J Appl Electrochem*, 2001, 31: 987–995.
- [5] LANTELME F, BENSLIMANE K, CHEMLA M. Electrochemical properties of solutions of  $\text{CrCl}_2$  and  $\text{CrCl}_3$  in molten alkali chlorides [J]. *J Electroanal Chem*, 1992, 337: 325–335.
- [6] NIE X M, DONG L Y, BAI C G, CHEN D F, QIU G B. Preparation of Ti by direct electrochemical reduction of solid  $\text{TiO}_2$  and its reaction mechanism [J]. *Transactions of Nonferrous Metals Society of China*, 2006, 16: 723–727.
- [7] ALEXANDER D T L, SCHWANDT C, FRAY D J. Microstructure kinetics of phase transformations during electrochemical reduction of titanium dioxide in molten calcium chloride [J]. *Acta Mater*, 2006, 54: 2933–2944.
- [8] WANG B, LIU K R, CHEN J S. Reaction mechanism of preparation of titanium by electro-deoxidation in molten salt [J]. *Transactions of Nonferrous Metals Society of China*, 2011, 21: 2327–2331
- [9] JIANG K, HU X H, MA M, WANG D H, QIU G H, JIN X B, CHEN G Z. Perovskitization-assisted electrochemical reduction of solid  $\text{TiO}_2$  in molten  $\text{CaCl}_2$  [J]. *Angew Chem Int Edit*, 2006, 45: 428–432.
- [10] YAN X Y, FRAY D J. Production of niobium powder by direct electrochemical reduction of solid  $\text{Nb}_2\text{O}_5$  in a eutectic  $\text{CaCl}_2$ – $\text{NaCl}$  melt [J]. *Metall Mater Trans B*, 2002, 33: 685–693.
- [11] WU T, XIAO W, JIN X B, LIU C, WANG D H, CHEN G Z. Computer-aided control of electrolysis of solid  $\text{Nb}_2\text{O}_5$  in molten  $\text{CaCl}_2$  [J]. *Phys Chem Chem Phys*, 2008, 10: 1809–1818.
- [12] SONG Q S, XU Q, KANG X, DU J H, XI Z P. Mechanistic insight of electrochemical reduction of  $\text{Ta}_2\text{O}_5$  to tantalum in a eutectic  $\text{CaCl}_2$ – $\text{NaCl}$  molten salt [J]. *J Alloy Compd*, 2010, 490: 241–246.
- [13] BARNETT R P, FRAY D J. Electro-deoxidation of  $\text{Ta}_2\text{O}_5$  in calcium chloride-calcium oxide melts [J]. *J Mater Sci*, 2014, 49: 4148–4160.
- [14] JIN X B, GAO P, WANG D H, HU X H, CHEN G Z. Electrochemical preparation of silicon and its alloys from solid oxides in molten calcium chloride [J]. *Angew Chem Int Edit*, 2004, 43: 733–736.
- [15] YIN H Y, XIAO W, MAO X H, WEI W F, ZHU H, WANG D H. Template-free electrosynthesis of crystalline germanium nanowires from solid germanium oxide in molten  $\text{CaCl}_2$ – $\text{NaCl}$  [J]. *Electrochim Acta*, 2013, 102: 369–374.
- [16] LI Q Y, DU J H, XI Z P. Preparation of zirconium by electro-deoxidation in molten salt [J]. *Transactions of Nonferrous Metals*

- Society of China, 2007, 17: 560–564.
- [17] MOHANDAS K S, FRAY D J. Electrochemical deoxidation of solid zirconium dioxide in molten calcium chloride [J]. Metall Mater Trans B, 2009, 40: 685–699.
- [18] DAI L, WANG S, LI Y H, WANG L, SHAO G J. Direct electrochemical preparation of CeCo<sub>5</sub> alloy from mixed oxides [J]. Transactions of Nonferrous Metals Society of China, 2012, 22: 2007–2013.
- [19] DAI L, WANG S, WANG L, YU Y, SHAO G J. Preparation of ZrMn<sub>5</sub> hydrogen storage alloy by electro-deoxidation in molten calcium chloride [J]. Transactions of Nonferrous Metals Society of China, 2014, 24: 2883–2889.
- [20] KILBY K T, JIAO S Q, FRAY D J. Current efficiency studies for graphite and SnO<sub>2</sub>-based anodes for the electro-deoxidation of metal oxides [J]. Electrochim Acta, 2010, 55: 7126–7133.
- [21] DAI L, LU Y, WANG X Y, ZHU J, LI Y H, WANG L. Production of nano-sized chromium carbide powders from Cr<sub>2</sub>O<sub>3</sub>/C precursors by direct electrochemical reduction in molten calcium chloride [J]. Int J Refract Met H, 2015, 51: 153–159.
- [22] VISHNU D S M, SANIL N, PANNEERSELVAM G, SUDHA R, MOHANDAS K S, NAGARAJAN K. Mechanism of direct electrochemical reduction of solid UO<sub>2</sub> to uranium metal in CaCl<sub>2</sub>-48mol%NaCl melt [J]. J Electrochem Soc, 2013, 160: 394–402.
- [23] QIU G H, MA M, WANG D H, JIN X B, HU X H, CHEN G Z. Metallic cavity electrodes for investigation of powders [J]. Electrochem Soc, 2005, 152: 328–336.
- [24] GAO P, JIN X B, WANG D H, HU X H, CHEN G Z. A quartz sealed Ag/AgCl reference electrode for CaCl<sub>2</sub> based molten salts [J]. J Electroanal Chem, 2005, 579: 321–328.
- [25] SCHWANDT C, FRAY D J. The electrochemical reduction of chromium sesquioxide in molten calcium chloride under cathodic potential control [J]. Z Naturforsch A, 2007, 62: 655–670.
- [26] VISHNU D S M, SANIL N, PANNEERSELVAM G, MAHATO S K, SOJA K V, MOHANDAS K S, NAGARAJAN K. Factors influencing the direct electrochemical reduction of UO<sub>2</sub> pellets to uranium metal in CaCl<sub>2</sub>-48 mol% NaCl melt [J]. J Electrochem Soc, 2013, 160: 583–592.
- [27] YAN X Y, FRAY D J. Electrochemical studies on reduction of solid Nb<sub>2</sub>O<sub>5</sub> in molten CaCl<sub>2</sub>-NaCl eutectic [J]. J Electrochem Soc, 2005, 152: 12–21.
- [28] LIU Z W, ZHANG H L, PEI L L, ZHU G J, XU H B, ZHANG Y. Investigations on reaction pathway and microstructure transformations during electrochemical reduction of Cr<sub>2</sub>O<sub>3</sub> in molten CaCl<sub>2</sub> [J]. J Electrochem Soc, 2016, 163: 781–786.
- [29] CHEN G Z, FRAY D J. Cathodic refining in molten salts: Removal of oxygen, sulfur, selenium from static and flowing molten copper [J]. J Appl Electrochem, 2001, 31: 155–164.
- [30] CHEN G Z, FRAY D J. A morphological study of the FFC chromium and titanium powders [J]. Transactions of the Institution of Mining and Metallurgy Section C, 2006, 115: 49–54.

## 在 CaCl<sub>2</sub>-NaCl 共融盐中直接电解制备金属铬

刘政伟<sup>1,2,3</sup>, 张红玲<sup>1,2</sup>, 裴丽丽<sup>1,2</sup>, 石义朗<sup>4</sup>, 蔡再华<sup>4</sup>, 徐红彬<sup>1,2</sup>, 张懿<sup>1,2</sup>

1. 中国科学院 绿色过程与工程重点实验室(中国科学院过程研究所), 北京 100190;
2. 中国科学院过程工程研究所 湿法冶金清洁生产国家工程实验室, 北京 100190;
3. 中国科学院大学, 北京 100049;
4. 湖北振华化学股份有限公司, 黄石 435001

**摘要:** 通过考察 800 °C 下固体三氧化二铬(Cr<sub>2</sub>O<sub>3</sub>)在等摩尔 CaCl<sub>2</sub>-NaCl 熔盐中的电还原过程, 得到一个更高效的金属铬制备工艺。利用循环伏安和恒电势电解法考察负载 Cr<sub>2</sub>O<sub>3</sub> 的金属空洞电极的电还原过程, 并考察影响 Cr<sub>2</sub>O<sub>3</sub> 电解速率和电解程度的重要电解参数。结果表明: CaCl<sub>2</sub>-NaCl 熔盐可用作直接电解 Cr<sub>2</sub>O<sub>3</sub> 制备金属铬的熔盐; 电解参数对电解产品质量影响明显。在最佳电解条件下, 得到氧含量为 0.5% (质量分数)的节支状金属铬产品, 且 X 射线衍射法没有检测到任何碳化铬存在。此外, CaO 较高的溶解度和 CaCr<sub>2</sub>O<sub>4</sub> 较快的晶体生长速率导致大颗粒片状 CaCr<sub>2</sub>O<sub>4</sub> 的生成。与纯 CaCl<sub>2</sub> 相比, 在 CaCl<sub>2</sub> 中添加 NaCl 可明显改变电解过程和产物形貌。

**关键词:** 电解; 金属铬; 氧化铬; CaCl<sub>2</sub>-NaCl 熔盐

(Edited by Wei-ping CHEN)